# Role of integrin adhesions in cellular mechanotransduction

Balcıoğlu, H.E.

# Chapter 3

# Integrin expression profile modulates orientation and dynamics of force transmission at cell-matrix adhesions [1]

[1] This chapter is based on: Hayri E Balcıoğlu, Hedde van Hoorn, Dominique M Donato, Thomas Schmidt and Erik HJ Danen, Integrin expression profile modulates orientation and dynamics of force transmission at cell-matrix adhesions. , *J. Cell. Sci.*, **128**, 1316-26 (2015)

## Abstract

Integrin adhesion receptors connect the extracellular matrix (ECM) to the cytoskeleton and serve as bidirectional mechanotransducers. During development, angiogenesis, wound healing, or cancer progression the relative abundance of fibronectin receptors, including α5β1 and αvβ3 changes, thus altering the integrin composition of cell-matrix adhesions. Here, we show that enhanced αvβ3 expression can fully compensate for loss of α5β1 and other β1 integrins to support outside-in and inside-out force transmission. α5β1 and αvβ3 each mediate actin cytoskeletal remodeling in response to stiffening or cyclic stretching of the ECM. Likewise, α5β1 and αvβ3 support cellular traction forces of comparable magnitudes and similarly increase these forces in response to ECM stiffening. However, cells using αvβ3 respond to lower stiffness ranges, more robustly reorganize their actin cytoskeleton in response to stretch, and traction forces are more randomly oriented in cells using αvβ3. Centripetal traction force orientation requires Rho kinase-Myosin II-mediated long stress fibers that are supported by α5β1. Thus, altering the relative abundance of fibronectin-binding integrins in cell-matrix adhesions affects spatiotemporal organization of force transmission.

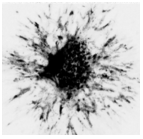

## 3.1 Introduction

Cells sense the mechanical properties of their surrounding environment and activate intracellular signaling cascades generating an elaborate response that plays a role in cell survival, proliferation, differentiation, and migration [1]. Cell-matrix adhesions are dynamic force responsive protein complexes that couple the extracellular matrix (ECM) to the cytoskeleton [2]. Within these adhesions, integrin α-β heterodimeric transmembrane receptors bind ECM proteins with their globular head domains and connect to the cytoskeleton via multi-protein interactions at their cytoplasmic tails [3]. Integrins transmit forces in a bi-directional manner: extracellular forces applied to the head domains enhance integrin activity and clustering, and trigger cell-matrix adhesion growth and cytoskeletal reorganization. Vice versa, actomyosin-mediated contractile forces cause strengthening of integrin-ECM binding [4–7].

Cell-matrix adhesions formed on fibronectin contain a mixture of different integrins, including α5β1 and αvβ3. When cells are stimulated to move or proliferate during development, angiogenesis, or tissue regeneration, shifts in the relative abundance of these fibronectin-binding integrins occur [8, 9]. Likewise, alterations in the abundance of α5β1 or αvβ3 take place during cancer progression [10]. Such changes will alter the integrin composition of cell-matrix adhesions and we and others have previously shown that this affects cytoskeletal organization, activity of Rho GTPases, and migratory behavior [11–13].

Using mouse embryonic stem (ES) cell-derived fibroblastic cells (GD25) and mouse embryo-derived neuroepithelial cells (GE11) lacking the common β1 subunit we have shown that re-expression of β1 (but not increased expression of β3 supporting a similar level of adhesion to fibronectin) stimulates RhoA-Rho kinase-mediated contractility and more random migration [11, 12]. Likewise, White et al. have shown that prevention of αvβ3 recycling in NIH3T3 cells thereby causing enhanced surface abundance of α5β1, stimulates Rho kinase-mediated contractility and random movement [14]. Conversely, Miao et al. demonstrated that expression of β3 integrins (but not increased expression of β1 integrins) in CHO cells that lack β3 causes enhanced RhoA-Rho kinase activity [13]. This may

suggest that the total amount of fibronectin-binding integrins is more relevant or that expression of both β1 and β3 integrins is needed for effective Rho-Rho kinase-mediated contractility. However, we showed that β3 knockout MEFs have no defect in RhoA-Rho kinase-mediated contractility and ectopic expression of β3 integrins does not further stimulate this pathway (whereas increased expression of β1 integrins does) [15]. Moreover, like expression of β1 integrins in β1 null cells; expression of α5 in α5 null mouse ES-derived fibroblastic cells also stimulates RhoA-Rho kinase-mediated contractility [15].

It has subsequently become clear that different integrins can mediate distinct signaling routes that support distinct aspects of mechanotransduction. Experiments using MEFs in which ligand-coated beads were used to pull on small integrin clusters have shown that α5β1 mediates adhesion strength whereas αvβ3 mediates cytoskeletal stiffening [16]. A recent study using pan-integrin knockout kidney fibroblasts reconstituted with αv, β1, or both subunits resulting in equimolar surface levels of α5β1 and/or αvβ3 and αvβ5 has provided further insight: α5β1-mediated adhesion indeed stimulates RhoA-Rho kinase signaling to activate Myosin II but αv integrins are required to support RhoA-mDia-mediated actin polymerization and these processes cooperate to regulate contractility [17]. Thus, the expression levels of α5β1, αvβ3, as well as other αv-integrins participating in fibronectin-binding (e.g. αvβ1 and αvβ6) in combination with the distinct signaling networks of integrin-associated proteins present in embryonic or ES-derived epithelial or fibroblastic cells, kidney cells, or CHO cells used in the above-mentioned studies ultimately determine the outcome of changes in the fibronectin-receptor repertoire for RhoA-mediated signaling and cytoarchitecture.

In this study we asked to what extent a shift from α5β1 to more αvβ3 expression, as often seen with angiogenesis, wound healing, or cancer progression, affects mechanotransduction. We used two independent cell systems in which adhesion to fibronectin is mediated mainly by α5β1 or by αvβ3 integrins resulting in comparable adhesion efficiency and compared the ability of such cells to i) sense and respond to extracellular forces (outside-in signaling), and ii) exert forces onto the ECM (inside-out signaling).

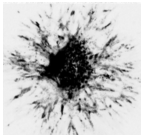

## 3.2 Results

### 3.2.1 Cells adhering through αvβ3 show more robust cytoskeletal reorganization in response to cyclic stretch as compared to cells using α5β1

To compare responses to extracellular forces we made use of GEβ1 and GEβ3 cells. These cells derived from β1 integrin chimeric mouse embryos lacked the common β1 subunit and were engineered to express human β1 or β3 subunits. Fluorescence-activated cell sorting (FACS) showed that ectopically expressed β1 and β3 led to high cell surface levels but these did not exceed endogenous levels observed in MDA-MB-435s human breast cancer cells (Figure S1C,D,G,I). GEβ1 and GEβ3 cells were previously shown to support adhesion to fibronectin-coated glass substrates with the same efficiency through either α5β1 or αvβ3, respectively [11]. The cells were transduced with mCherry-LifeAct for actin imaging (Figure S1E,F,I,J) and plated on a fibronectin-coated Poly (DiMethyl)Siloxane (PDMS) membrane and subjected to uniaxial, cyclic stretch first at 10% 1 Hz for 2 hours, then at 20% 1 Hz for 1 hour (Figure 3.1A). Incubation with integrin blocking antibodies confirmed that, like fibronectin-coated glass substrates, GEβ1 and GEβ3 adhered to fibronectin-coated PDMS substrates mainly through α5β1 and αvβ3, respectively (Figure S2H). Upon cyclic stretch, both GEβ1 and GEβ3 cells showed a gradual decrease in cell-spreading area with the two subsequent stretching regimes. The total actin filament length showed the same trend for GEβ1 but for GEβ3 cells the total filament length already approached a minimum value at 10% stretch and showed only a slight additional decrease after subsequent 20% stretching (Figure 3.1B-E).

PDMS membranes, coated with fluorescent beads or stamped with patterned fluorescently labeled fibronectin were used to characterize the strain field over the membrane, the dynamic strain in the imaging field, and to determine the angle of minimal strain (Figure 3.1A; Figure S2A-D). GEβ1 cells oriented their F-actin towards the minimal strain direction (∼60° to the macroscopic strain) following the 10% stretch regime but this response was lost during the subsequent, second regime of 20% stretch (Figure 3.1F,H). GEβ3 cells subjected to the first stretch regime showed a more prominent actin filament orientation towards the minimal strain direction and this response was maintained during the 20% stretch regime (Figure 3.1G,H).

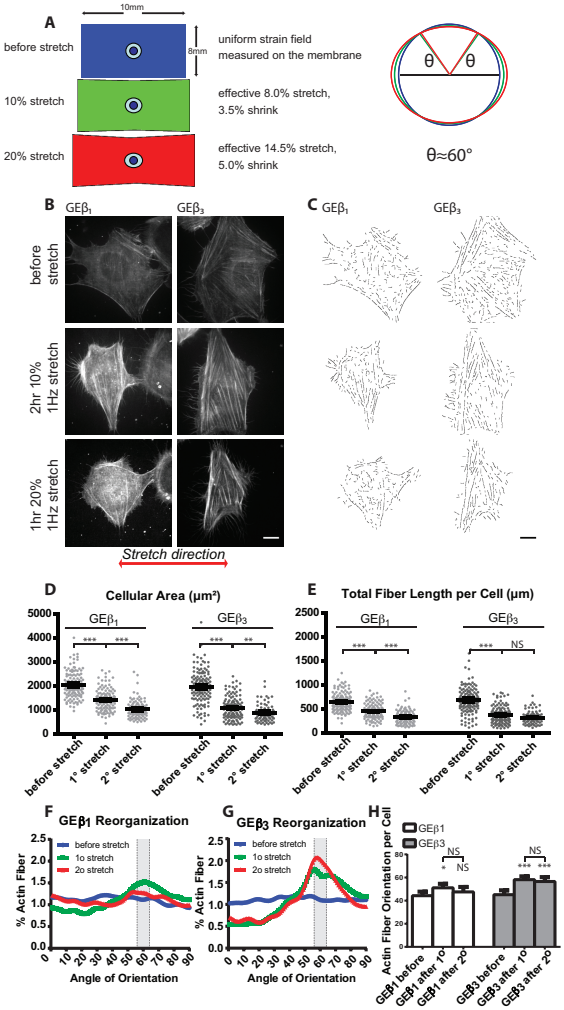


## Figure 3.1

***Cells expressing αvβ3 integrins more effectively reorganize their cytoskeleton upon cyclic stretch.*** *(A) Stretch regimes used during the experiment. Driving the piezo controllers with 10%/20% displacement resulted in 8%/14.5% stretch on the PDMS membrane in the direction of the displacement, and 3.5%/5% shrink in the perpendicular direction. This resulted in a minimal strain angle of ∼60°. (B) mCherry-LifeAct-transduced GEβ1 and GEβ3 cells respond to 2 step cyclic stretch. (C) Characterization of actin organization. (D,E) Quantification of cellular spread area (D) and total actin filament length (E). Mean 95% clearance level of >75 cells from 3 independent experiments. (F,G) Angular organization of actin filaments averaged over all GEβ1 (F) or GEβ3 (G) cells measured. Measured angle of orientation of actin filaments is relative to stretch direction. Grey bar indicates region of minimal strain. (H) Average actin filament orientation per cell, mean ± 95% clearance level of >75 cells from 3 independent experiments. NS, p>0.05; *,p<0.05; **, p<0.005; ***, p<0.0005 according to Mann-Whitney test. Scale bar is 10 μm.*

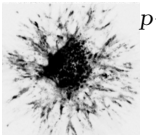

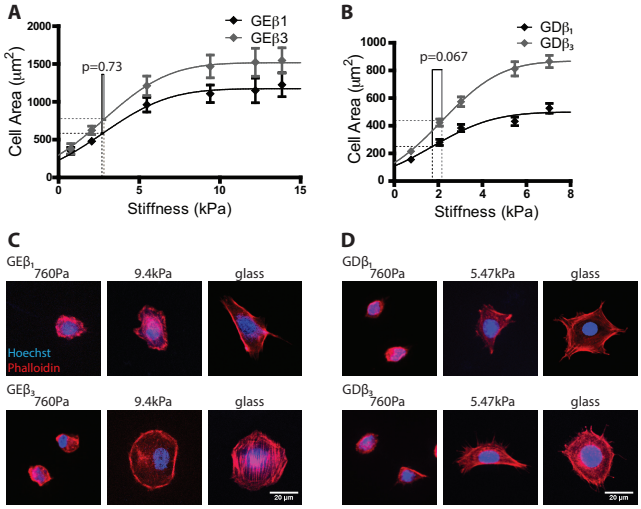


**Figure 3.2**
***Cells respond to increased substrate stiffness by increased spreading irrespective of the integrin engaged.*** *(A,B) Quantification of cellular spread area of GEβ1 and GEβ3 cells (A) or GDβ1 and GDβ3 cells (B) over measured rigidities and cumulative Gaussian distribution model fitted. Mean ±95% clearance level is shown. >100 cells were measured from 3 different experiments (except at 760 Pa for GEβ1 and GEβ3 cells where more than 60 cells were measured from a single experiment). P values were calculated by comparing the halfway points of the cumulative Gaussian fits with an F-test. (C,D) Representative images for A and B. Scale bar is 20 μm.*

These findings indicate that cells adhering mainly through α5β1 or αvβ3 integrins can both sense cyclic ECM strain and trigger actin cytoskeleton remodeling. However, high expression of αvβ3 allows cells to more effectively reorient their cytoskeleton in the direction of minimal strain and maintain this orientation at high strain rates.

### 3.2.2 Cells expressing α5β1 or αvβ3 each support cell spreading in response to substrate stiffening

Next, we seeded GEβ1 and GEβ3 cells onto fibronectin-crosslinked polyacrylamide (PAA) gels with shear moduli varying between 760 Pa and 13.4 kPa (Figure S2F,G). Incubation with integrin blocking antibodies confirmed that, like fibronectin-coated glass and PDMS substrates, GEβ1 and GEβ3 adhered to fibronectin-crosslinked PAA substrates mainly

through α5β1 and αvβ3, respectively (Figure S2I). Both cell types showed a gradual increase in cell spreading area with increasing stiffness (Figure 3.2A,C). Similar findings were obtained using the GD25 cell line derived from β1 null ES cells where expression of human β1 or β3 subunits supports adhesion to fibronectin with the same efficiency through α5β1 or αvβ3, respectively [11] and had comparable surface expression levels of these integrins as MDA-MB-435s cells (Figure S1A,B,H,I). Parenthetically, for GD cells lower stiffness ranges were used as compared to those used for the GE cell lines since full cell spreading was already observed on softer substrates for this cell type. Again, cell-spreading area increased with increasing stiffness over the range of stiffnesses tested for cells adhering through either of these integrins (Figure 3.2B,D). Non-linear fitting using a cumulative Gaussian distribution (Figure S3A) showed that despite having significantly different response curves (Figure S3B-D) the estimated half response stiffness ($E_{1/2}$) was not integrin specific (Figure 3.2A,B).

### 3.2.3 Cells adhering through αvβ3 form cell-matrix adhesions at lower substrate stiffness compared to cells adhering through α5β1

Similar to cellular area, the number of peripheral cell-matrix adhesions increased with increasing stiffness for all cell lines. For GEβ3 and GDβ3 cells the number of peripheral cell-matrix adhesions reached its maximum at intermediate stiffness with an elastic modulus of 9.4 and 5.47 kPa, respectively (Figure 3.3A,B,D; Figure S3J). By contrast, the number of cell-matrix adhesions in GEβ1 and GDβ1 cells showed a more gradual increase over the entire range of stiffnesses tested (Figure 3.3A,B,C; Figure S3I). The half response stiffness ($E_{1/2}$) was also significantly lower for cells using αvβ3, as compared to that for cells using α5β1 (Figure 3.3A,B; Figure S3B,E,F). The average cell-matrix adhesion size did not show the same gradual response to rigidity: once adhesions were formed, they reached similar sizes irrespective of the ECM stiffness (Figure 3.3C,D; Figure S3G-J).

Taken together, these findings demonstrate that cells expressing α5β1 and αvβ3 can each sense - and respond to - variations in substrate stiffness but αvβ3 supports cell-matrix adhesion formation more readily at a lower stiffness.

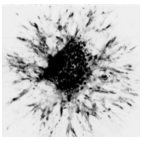

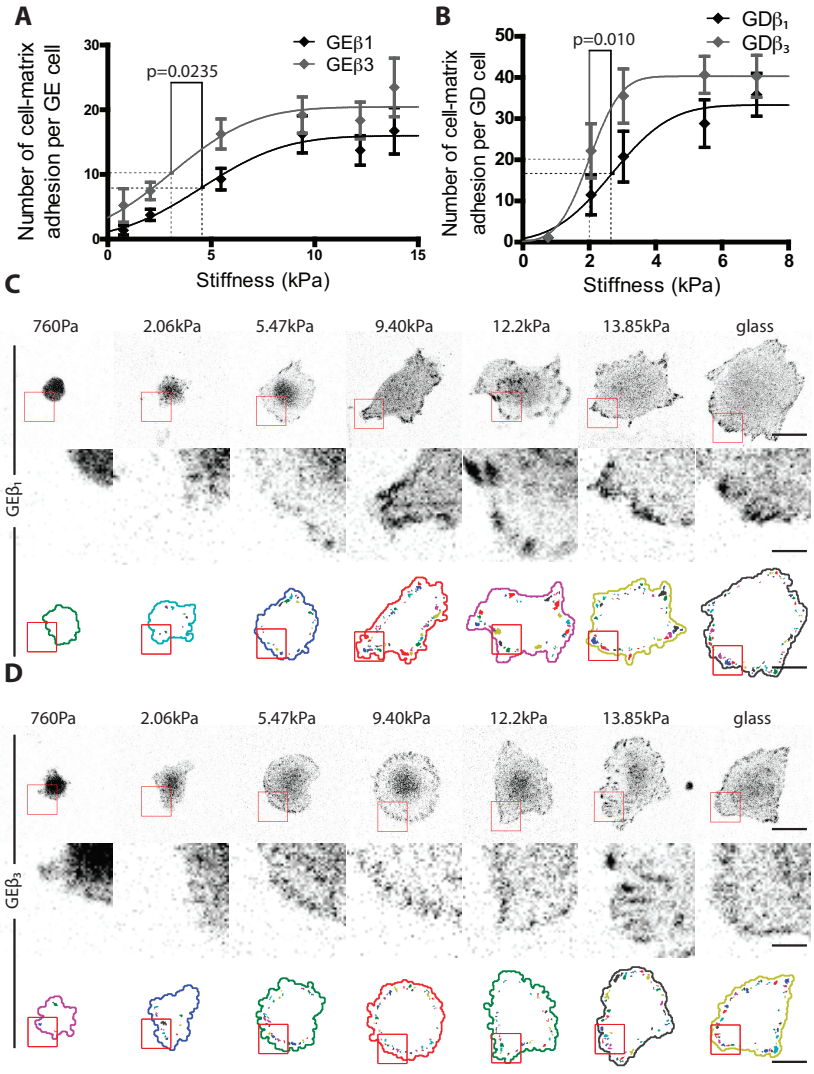


**Figure 3.3**

***Number of cell-matrix adhesions increases with increasing stiffness in an integrin-controlled manner.*** *(A,B) Quantification of number of peripheral cell-matrix adhesions of GEβ1 and GEβ3 cells (A) or GDβ1 and GDβ3 cells (B) over measured rigidities and fitted cumulative Gaussian distribution function. In all graphs, mean ±95% clearance level is shown and at least 20 cells were measured over 3 different experiments (except for 760 Pa for GEβ1 and GEβ3 cells where results of one experimental replica is shown). P values were calculated by comparing the halfway points of the cumulative Gaussian fits (A,B) with F-test. (C,D) Representative images of Paxillin (top), zoomed in region of the boxed area (middle) and adhesions detected by the automated analysis algorithm (bottom). Scale bar is 20 µm (5 µm for zooms).*

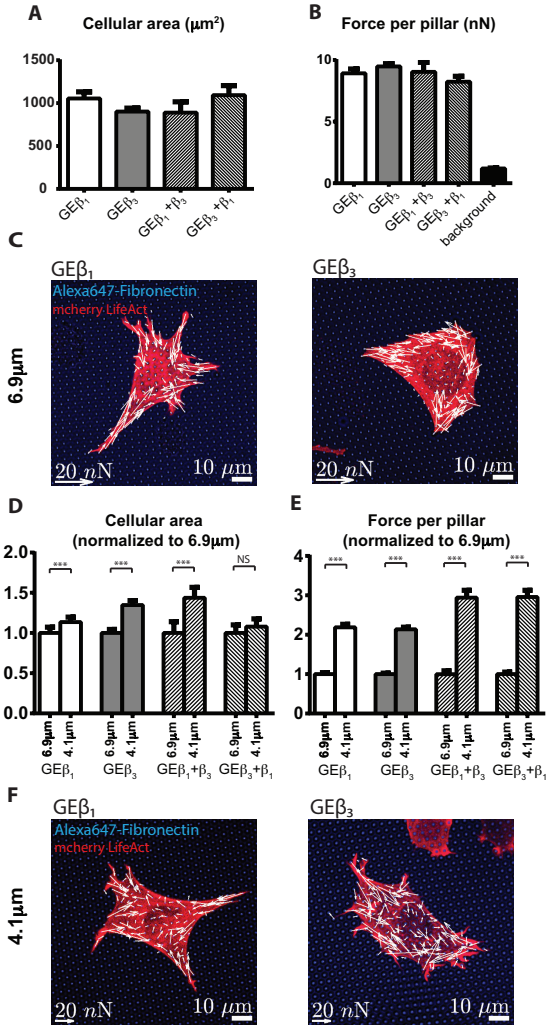


## Figure 3.4

***Cellular traction force generation is similar for cells using α5β1 or αvβ3 integrins.*** *(A-B) Bar plots of cellular spread area and force per pillar of the indicated cell lines seeded on 6.9 μm PDMS pillars. Background indicates forces measured in areas not covered by cells. (C) Representative images from A,B; white arrows indicate magnitude and direction of forces measured. Scale bar, 20 nN/10 μm. (D,E) Bar plots of cellular spread area and force per pillar of the indicated cell lines seeded on 4.1 μm PDMS pillars, relative to measurements on 6.9 μm pillars. In all graphs, mean ±95% clearance level is shown and at least 30 cells were measured over 3 different experiments. (F) Representative images from D,E. White arrows and scale bars as in C.*

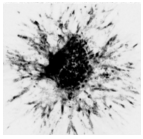

### 3.2.4 Cells adhering through α5β1 or αvβ3 each mediate traction forces that are regulated in response to altered substrate rigidity

Having examined the consequences of expression of either α5β1 or αvβ3 for outside-in cellular responses to extracellular forces, we next investigated whether these integrins differed in their ability to mediate inside-out cellular traction forces onto the ECM. Therefore, mCherry-LifeAct-expressing GEβ1 and GEβ3 cells were seeded on fibronectin-stamped PDMS micropillars of 6.9 µm height (bending stiffness of 16 nN/µm). Cell spreading on these micropillars as well as the average force per pillar was similar for both cell lines (Figure 3.4A-C). This indicated that β1 integrins were not required for the generation of traction forces in cells where αvβ3 levels are sufficiently high to compensate for adhesion, despite earlier reports pointing to a critical role for β1 integrins [16, 17]. To address whether expression of β1 integrins might further increase traction forces in GEβ3 cells we plated GEβ1+β3 and GEβ3+β1 cells on 6.9 µm fibronectin-stamped micropillars. However, comparable cell spreading and forces were measured for these cells as observed for GEβ1 and GEβ3 cells (Figure 3.4A,B). Together, these findings indicate that traction forces can be generated irrespective of the type of fibronectin-binding integrin expressed.

We next analyzed the ability of these cells to increase traction forces in response to increased substrate stiffness. Plating cells on shorter pillars (4.1 µm height; bending stiffness of 66 nN/µm) led to increased cell spreading and to ∼2-fold increase in traction forces, irrespective of the integrin used (Figure 3.4D-F). The increase in traction force was ∼3-fold for GEβ1+β3 and GEβ3+β1 cells indicating that the total amount of fibronectin-binding integrins may determine the magnitude of the response (Figure 3.4E). The 2-fold increase in response to substrate stiffening was maintained for GEβ1 and GEβ3 cells in post-fixation samples and GDβ1 and GDβ3 cells each showed a similar response although the magnitude of the response to stiffening was lower for GDβ3 cells (Figure S4A-C). In addition, a similar, albeit somewhat stronger increase in traction forces upon seeding on shorter pillars was observed for NIH3T3 cells that bind to fibronectin via both α5β1 and αvβ3 [18] (Figure S4A,B). Lastly, having established that initial adhesion to fibronectin-coated PDMS involved α5β1 for GEβ1 cells and αvβ3 for GEβ3 cells (Figure S2H), we analyzed the potential role of αv integrins in the traction forces exerted

by these cells. As expected, αv integrin-blocking antibodies decreased force application by GEβ3 cells but they did not affect traction forces in GEβ1 cells, indicating that α5β1 was the major integrin responsible for force application on fibronectin in GEβ1 (Figure S4D-F).

These results indicate that cells are able to exert traction forces and respond to increased ECM stiffness by enhanced force application, irrespective of the type of fibronectin receptor engaged. Notably, the approximated shear modulus of 3.87 and 15.7 kPa of these long and short pillars (see Materials and methods section), was within the outside-in sensing regimes tested using PAA substrates (Figures 3.2, 3.3).

### 3.2.5 Cells adhering through α5β1 preferentially support centripetal force application and long actin filaments in an actomyosin contractility-dependent manner

Cells expressing α5β1 or αvβ3 show distinct organization of the actin cytoskeleton and cell-matrix adhesions with α5β1 supporting predominantly concave cortical actin structures [11, 12] (Figure 3.2C-D). We hypothesized that the morphology supported by α5β1 was related to more centripetally oriented forces exerted at cell-matrix adhesions. In order to investigate this, we analyzed the centripetally oriented force fraction, i.e. forces directed towards the cell center compared to the total force. Live measurement of traction forces on 6.9 µm and on 4.1 µm pillars showed that the centripetal force fraction in GEβ1 cells was slightly but significantly higher than that observed in GEβ3 cells (Figure 3.5A, left panel). The centripetal force fraction in GEβ1+β3 and GEβ3+β1 cells was comparable to that in GEβ1 cells. The higher centripetal force fraction in β1-expressing cells was also observed in post-fixation samples of GDβ1, GDβ3, GEβ1, and GEβ3 cells on 4.1 µm pillars (Figure 3.5A, middle panel).

We measured cortical actin filament lengths in GEβ1 and GEβ3 cells on 4.1 µm pillars and noticed that higher centripetal force orientation in GEβ1 correlated with longer average cortical actin filament length (Figure 3.5B,C). This suggested that the longer actin filaments in α5β1 expressing cells, rather than shorter actin cables in αvβ3 expressing cells, supported the centripetal orientation of forces. We and others have previously observed that α5β1 supports Rho kinase-mediated actomyosin contractility [11, 12, 14, 17] and we tested whether Rho kinase signaling was involved in the centripetal orientation of applied forces. Indeed, inhi-

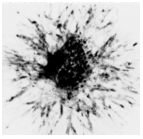

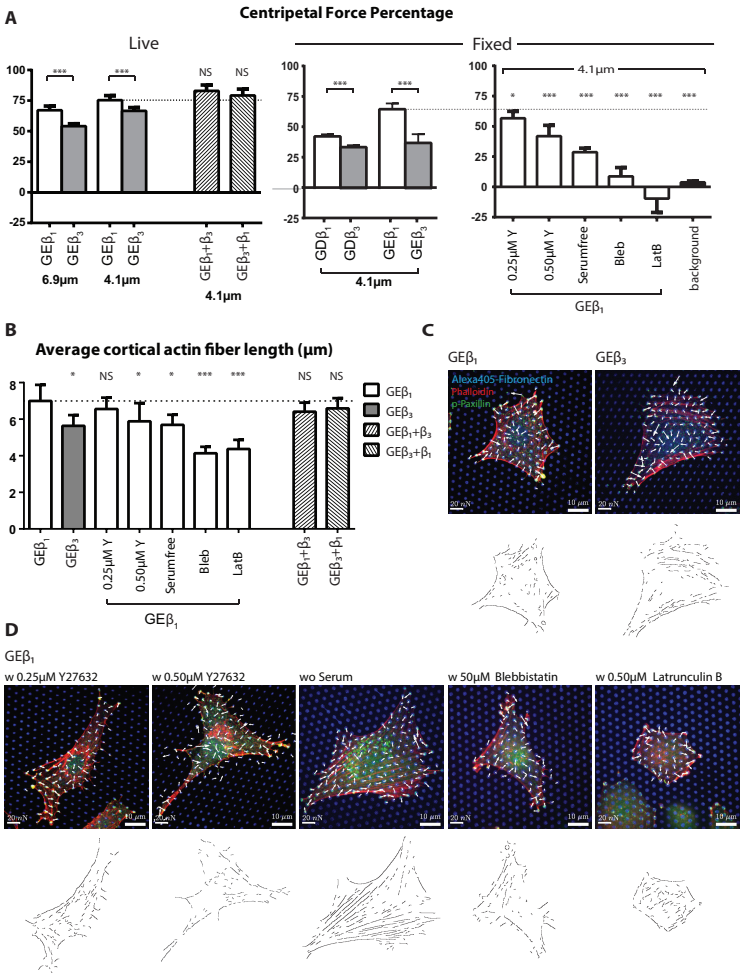


## Figure 3.5

***Higher centripetal force fraction in cells using α5β1 correlates with longer cortical actin filaments through Rho kinase-Myosin activity.*** *(A) Bar plots showing percentage centripetal force for the indicated cell lines on 6.9 µm and 4.1 µm PDMS pillars determined by live microscopy (left graph) or post-fixation analysis (middle and right graphs). Treatments in the right graph are 0.25 µM Y and 0.5 µM Y, Y27632 concentrations; bleb, 50 µM blebbistatin; LatB, 0.5 µM Latranculin B. Background indicates forces measured in areas not covered by cells. (B) Bar plots of average cortical actin filament length of the indicated cell lines on 4.1 µm PDMS pillars. Indicated treatments as in A, right graph. In all graphs mean ±95% clearance level is shown and at least 15 cells were measured over 3 different experiments. Indicated P values are compared to untreated β1 expressing cells (marked by dotted lines); NS, $p>0.05$; *, $p<0.05$; **, $p<0.005$; ***, $p<0.0005$ according to Mann-Whitney test. (C, D) Representative images (top) and extracted actin cytoskeleton (bottom) for control (C) and treatment conditions (D). White arrows indicate magnitude and direction of forces measured. Scale bar, 20 nN/10µm.*

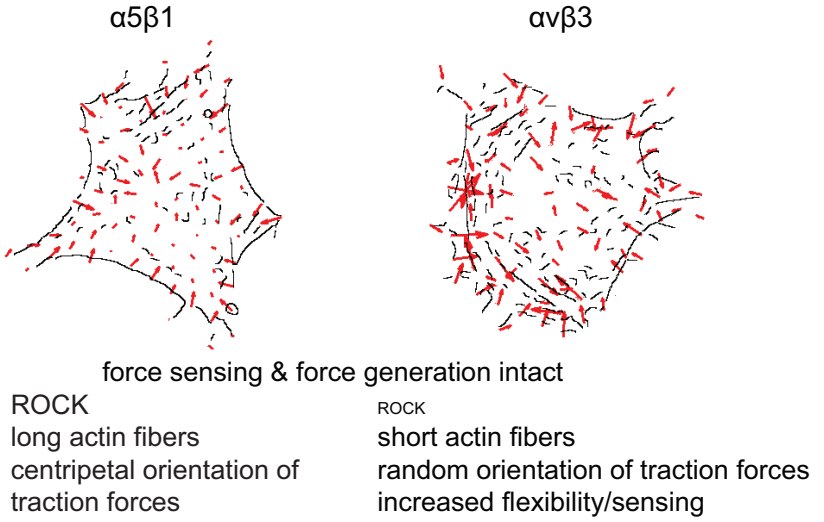


**Figure 3.6**
***Model for integrin regulated mechanotransduction.*** *Both α5β1 and αvβ3 integrins are able to support sensing and responding to mechanical cues from the environment (outside-in signaling) and to mediate force generation onto the ECM (inside-out signaling). Rho kinase-Myosin-mediated long actin filaments are supported by α5β1 integrins and allow cells to apply centripetally oriented forces. Shorter actin filaments in αvβ3 expressing cells support more randomly oriented traction forces and may provide flexibility to reorganize the actin cytoskeleton in response to mechanical cues from the environment. Potential roles for alternative αv integrins (e.g. αvβ1 and αvβ6) are not tested here but may modulate the outcome of shifts in expression of α5β1 and αvβ3.*

bition of Rho kinase or withdrawal of serum (containing lysophosphatidic acid, a known stimulator of Rho-Rho kinase signaling [19]) reduced the centripetal orientation of force (Figure 3.5A right panel). These treatments also, though less effectively, reduced the average cortical actin filament length in GEβ1 to the level observed for GEβ3 (Figure 3.5B,D). Likewise, treatment of GEβ1 cells with the Myosin-II inhibitor blebbistatin or disruption of the actin cytoskeleton with latrunculin B left only short actin cables intact and abolished the centripetal force orientation (Figure 3.5B,D).

Together, these data show that even though traction forces mediated by α5β1 and αvβ3 (possibly supported by other fibronectin-binding αv integrins) are similar in magnitude; orientation of these forces is dif-

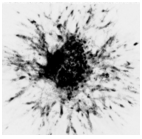

ferentially regulated. This difference is related to long-range cortical actomyosin fibers supported by Rho kinase and Myosin-II in the context of α5β1 versus shorter actin cables in the context of αvβ3 (Figure 3.6).

## 3.3 Discussion

Cell matrix adhesions couple the ECM to the F-actin network and are regions for force transmission, allowing cells to adapt to the mechanical properties of the environment and to exert forces needed to remodel their environment. Our findings demonstrate that cell matrix adhesions can function as bi-directional force transducers irrespective of whether they contain α5β1 (and very little αvβ3) or αvβ3 (in the absence of any β1 integrins). It should be noted that a contribution of alternative αv integrins such as αvβ5, αvβ6, αvβ8 or, in the case of cells expressing β1 integrins, αvβ1 cannot be fully ruled out in our study. Integrins α5β1 and αvβ3 have been shown to play distinct roles in adhesion strengthening and actin cytoskeletal stiffening in integrin clusters under force [16]. Our findings show that this does not translate into reduced force application by cell-matrix adhesions in the absence of α5β1 or ineffective F-actin reorganization when αvβ3 expression is low; provided there is compensation through enhanced expression of αvβ3 or α5β1, respectively. Cells expressing either α5β1 or αvβ3 each respond to cyclic substrate stretching and each can sense variations in substrate stiffness and accordingly trigger cell spreading and cell matrix adhesion formation. Likewise, both integrins allow cell matrix adhesions to apply traction forces onto the ECM and respond to increased stiffness with enhanced force application.

Nevertheless, the manner in which force transduction is dynamically organized in cells expressing either of these integrins does differ. Our findings indicate that cells expressing αvβ3 form cell matrix adhesions more effectively at lower substrate stiffnesses and more robustly reorganize their actin cytoskeleton to find the minimal strain in response to substrate stretching. It has been reported that substrate stretching triggers Phosphatidylinositol-4,5-bisphosphate 3-kinase-(PI3K)-mediated αvβ3 activation, which in turn stimulates cellular responses including c-Jun N-terminal kinase(JNK) activation [20]. It will be of interest to explore whether such a mechanism underlies the effective cytoskeletal reorganization observed in cells expressing high levels of αvβ3. The emergence of αvβ3, which is frequently observed during active processes such as an-

giogenesis or cancer invasion [10] may provide endothelial or tumor cells in these cases with enhanced flexibility to adapt their cytoarchitecture to ECM properties and activate cellular signaling in soft environments.

Our findings indicate that cells using α5β1 or αvβ3 respond to substrate stiffening by cell spreading, cell matrix adhesion formation, and by applying more force to the substrate. It has been demonstrated that αv-integrins support coupling of RhoA activity to mDia, which drives actin polymerization [17]. Unlike that study, our experiments do not test such a role for fibronectin-binding αv-integrins in mechanotransduction; αv-integrins are expressed in all cell variants tested in our study (αvβ1 and others in GEβ1 and GDβ1; αvβ3 and others in GEβ3 and GDβ3). Unlike earlier reports [16, 17], we do not observe a marked deficiency in traction force induction by cells lacking β1 integrins when αvβ3 is expressed at sufficient levels to fully rescue the adhesion defect. Notably, expression levels in our study are comparable to endogenous levels of β1 or β3 found in cancer cells. The role of fibronectin-binding integrins in traction force generation appears to differ for different cell types. Besides variations in the profile of αv integrins for which the distinct roles in cytoskeletal organization are poorly understood; the integrin-associated signaling complex including Rho GTPases and their upstream regulators and downstream effectors may differ considerably in the variety of cell types used in different studies. This makes a direct comparison of different studies exploring integrin-mediated control of cytoskeletal organization and mechanotransduction difficult.

It has been reported that extracellular stimuli leading to activation of α5β1 but not those causing activation of αvβ3 can trigger cell traction forces [21]. The authors measured total force per cell; a parameter that is sensitive to effects on cell spreading area. Instead, here we determined force per pillar, which is independent of cell spreading area, and show that the induction of traction forces in response to extracellular stiffening can occur through both α5β1 and αvβ3. The report from Lin et al. and our current study differ in the stimuli that are used (antibody-mediated integrin activation versus substrate stiffening through pillar shortening) and in the cell types that are tested, which may regulate force transmission differently. Our findings show that both integrins can be used by cells to sense alterations in the physical properties of the environment and to respond to such changes by modulation of traction forces exerted onto the ECM.

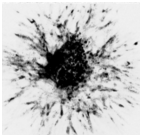

Rather than a role for α5β1 in force generation per se, which we show can be compensated for by enhanced expression of αvβ3 in complete absence of β1 integrins, we demonstrate that the orientation of forces is determined by the absence or presence of α5β1. This integrin allows cells to maintain contractile forces directed to the center of the cell and in its absence, forces become more randomly oriented. The ability of α5β1 to induce Rho kinase-Myosin-II-mediated signaling as demonstrated by us and others [11, 12, 14, 17] is important in this respect. We show that it allows cells to form long actin filaments that may support long-range force organization.

In conclusion, our findings show that both α5β1 and αvβ3 integrins support force sensing and force generation, but α5β1 predominantly mediates centripetally-oriented traction forces that are supported by Rho kinase and Myosin-II-mediated long actin filaments. By contrast, the shorter actin cables that are supported by αvβ3 allow more random force application and may provide cells with increased actin cytoskeletal flexibility, allowing them to more dynamically respond to mechanical cues (Figure 3.6). This may be particularly relevant in processes in which tissues go through extensive physical remodeling such as embryonic development, angiogenesis and cancer progression where emergence of αvβ3 has been documented.

## 3.4 Materials and methods

### 3.4.1 Fluorescence-activated cell sorting (FACS) analysis

For FACS, cells were detached using trypsin/EDTA and integrin surface expression levels were determined using primary antibodies (for human integrin β1, AIIB2, Developmental Studies Hybridoma Bank, Iowa City, IA, USA and for human integrin β3, 23CA, Santa Cruz Biotechnology, Inc., Dallas, TX, USA) and fluorescence-conjugated secondary antibodies (Alexa488-conjugated anti-rat or anti-rabbit, both from Invitrogen/Fisher Scientific, Breda, The Netherlands) and analyzing on a FACSCanto (Becton Dickinson, Breda, The Netherlands).

### 3.4.2 Cell culture

GD25 and GE11 cell lines expressing either α5β1 or αvβ3 or both integrins have been described previously [11, 12] and were selected for integrin ex-

pression using bulk FACS (Figure S1). Cells were cultured in medium (DMEM; Dulbecco's modified Eagle's Medium, Invitrogen/Fisher Scientific) supplemented with 10% fetal bovine serum (HyClone, Etten-Leur, The Netherlands), 25 U/ml penicillin and 25 µg/ml streptomycin (Invitrogen/Fisher Scientific cat. # 15070-063). For visualization of the actin cytoskeleton, cells were transduced using a lentiviral mCherry-LifeAct cDNA expression vector (provided by Dr. Olivier Pertz, University of Basel, Basel, Switzerland), selected in medium containing 2 µg/ml puromycin (Acros Organics/Fisher Scientific cat. # 227420500), and bulk sorted for mCherry expression using FACS (Figure S1C-F,J). MDA-MB-435s human breast cancer cells were cultured in RPMI medium 1640 (Invitrogen/Fisher Scientific) supplemented with 10% fetal bovine serum, 25 U/ml penicillin and 25 µg/ml streptomycin. NIH3T3 cells were cultured in DMEM supplemented with 10% newborn calf serum, 25 U/ml penicillin and 25 µg/ml streptomycin.

### 3.4.3 Cyclic cell stretching

An in-house made, piezo-driven, uniaxial stretcher was used to apply cyclic stretch with defined frequency, duration and displacement, on cells adhered to a fibronectin-coated PDMS membrane. Membranes were generated by pipetting well mixed PDMS (Sylgard 184, Dow Corning, Midland, MI, USA) at 1:10 (crosslinker:prepolymer) ratio inside a glass mold passivated with trichloro (1H,1H,2H,2H-perfluorooctyl)silane (Sigma Aldrich, Zwijndrecht, The Netherlands) and incubating for 20 hours at 110°C. This membrane was mounted on the stretcher, coated with 10 µg/mL fibronectin (Sigma Aldrich cat. # F1141) in phosphate buffered saline (PBS) and cells were seeded and incubated overnight in complete medium at 37°C and 5% $CO_2$ to allow full spreading. The stretcher was then mounted on a spinning-disk confocal microscope (see microscopy), and was kept at 37°C by a stand-alone single loop temperature controller (#3216, InvensysEuroterm, Alphen aan den Rijn, The Netherlands) connected to heaters and a thermo-coupler. LabVIEW (National Instruments, Austin, TX, USA) scripts developed by Wim Pomp (Physics of Life Processes, Kamerlingh Onnes-Huygens Laboratory, Leiden University, Leiden, the Netherlands) and provided by the manufacturer of the controller unit (MCS-3D, SmarAct, Oldenburg, Germany) were used to drive two independent piezo motors (SLC2430s, SmarAct) that allowed uniaxial stretching. Images were collected before

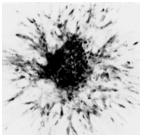

stretch application, after 2 hours of 10%, 1 Hz stretching and after a subsequent 1 hour of 20% 1 Hz stretching.

### 3.4.4 Characterization of stretcher strain field

The strain field was quantified with help from Donato Civita (Physics of Life Processes, Kamerlingh Onnes-Huygens Laboratory, Leiden University, Leiden, the Netherlands) by stretching a membrane with a micro-contact printed hexagonal lattice of fluorescent dots (Alexa647, Invitrogen). Two-dimensional image cross-correlation provided a deformation field over the entire substrate (Figure S2A). Differentiation using the Lagrangian strain tensor yielded the strain on every position on the substrate. The strain was 0.43% in the x-direction and -0.18% in the y-direction for every 0.5% externally applied static strain. These results were homogeneous and reproducible over the entire substrate within a strain measurement error of 0.01%.

For characterizing strain at cyclic stretch conditions, a PDMS membrane with fluorescent beads dried on top was used and the piezo motors were run at 10% or 20% displacement at 0.01Hz and a stack of images was obtained every 2 or 3 seconds, respectively to get the in-focus image and calculate strain. A macroscopic strain of 10% and 20% resulted in 8.0% and 14.5% strain, respectively, on the central area of the membrane along the direction of global strain. The substrate showed 3.5% and 5.0% shrinkage, respectively, in the perpendicular direction (Figures 3.1A, S2A-D). Based on these measurements we calculated that the minimal strain was at 57° and 60°, respectively relative to direction of macroscopic strain.

### 3.4.5 PAA substrates

PAA gels on 12 mm coverslips were made according to specifications adapted from [22]. Briefly, autoclaved 12 mm coverslips (Thermo Fisher cat. #360302) were cleaned with 0.1 M NaOH, and then rendered hydrophilic by incubating with 0.5% 3-aminopropyltrimethoxysilane (Sigma-Aldrich cat. # 281778). The coverslips were then washed thoroughly with sterile distilled water and incubated in 0.5% glutaraldehyde (Sigma-Aldrich cat. # G6257). Upon removal of the glutaraldehyde, the coverslips were left overnight to dry in a laminar flow cabinet. Coverslips of 10 mm diameter (Thermo Fisher cat. #360301) were rendered hy-

drophobic by incubating with a solution of 10% Hydrocarbon-Soluble Siliconizing Fluid (Surfa Sil; Thermo Fisher, cat. # TS-42800) in chloroform. Surfa Sil-treated coverslips were washed in 100% chloroform and then washed twice with methanol before being left overnight in a laminar flow cabinet to dry. PAA solutions were made with compositions of 7.5% acrylamide (Biorad cat. # 161-0141, Veenendaal, The Netherlands) and varying concentrations (0.01%, 0.03%, 0.05, 0.1%, 0.15%, 0.2%, 0.3% and 0.5%) of bis-acrylamide (Biorad cat. # 161-0200) to a final volume of 1 mL. To this solution 1.5 µL of TEMED (Thermo Fisher cat. # 17-1312-01) and 5 µL of 10% ammonium persulfate were added to start polymerization. 10 µL of this final solution was applied to the middle of each 12 mm coverslip. The 10 mm coverslips were then placed on top of this solution to form a sandwich and left to polymerize for 30 minutes. 50 mM (4-(2-hydroxyethyl)-1-piperazineethanesulfonic acid) HEPES was added and after 15 minutes the top coverslips were removed and the gels were washed once with 50 mM HEPES. PAA gels were activated with an organic crosslinker by removing HEPES and submerging gels in a solution of 0.5 mM sulfosyccinimidyl-6-[4-azido-2-nitrophenylamino]hexanoate (Thermo Fisher, cat. # 22589) and 50 mM HEPES and placing under UV light (Philips HP3114, Eindhoven, The Netherlands). This step was repeated a second time after a wash with 50 mM HEPES. The gels were then washed twice with 50 mM HEPES and incubated overnight at 4°C in 10 µg/mL fibronectin (Sigma Aldrich cat. # F1141) in PBS. After washing with PBS, gels were allowed to equilibrate for one hour in complete culture medium at 37°C before seeding with 25,000 cells/well in complete medium. Cells were allowed to adhere and spread before fixation by incubating for two hours at 37°C and 5% $CO_2$.

### 3.4.6 Analysis of stiffness of PAA gels by rheology

Rheology experiments were performed with a stress-controlled rheometer (Physica MCR 501; Anton Paar, Graz, Austria) with assistance from Karin A. Jansen and Gijsje H. Koenderink (Biological Soft Matter Group, FOM Institute AMOLF, Amsterdam, The Netherlands) as previously described [23]. Briefly the PAA gel was polymerized at 21°C between a steel cone and plate (40 mm diameter, 1°) and shear storage modulus was recorded in real time during the polymerization (approximately 1 hour) by applying a small-amplitude oscillatory strain with

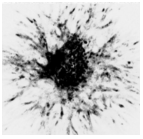

amplitude 0.5% and frequency 3.14 rad/s. After polymerization, PBS was added to the measuring chamber and the system was brought to 37°C while monitoring the shear storage modulus. The measured shear loss modulus was more than two orders of magnitude smaller than the storage component, hence was ignored.

### 3.4.7 PAA and PDMS adhesion assay

GEβ1 and GEβ3 cells were first incubated on ice with blocking antibodies targeting integrin mouse-α5 (cat# MAB1984, Millipore, CA, USA), mouse-αv (cat# 552299 Becton Dickinson, Breda, The Netherlands), human-β1 (AIIB2) and human-β3 (23CA) for 30 minutes and then seeded on PAA gels (stiffness of 12.2 kPa) for 1 hour or on PDMS blocks (1:10 crosslinker:prepolymer ratio) for 30 min at 37°C and 5% $CO_2$ fixed with formaldehyde and cells on 6-10 different fields of view per condition were counted.

### 3.4.8 Assays using PDMS micropillars

Micropillars were used for cellular traction force measurements according to methodology described previously [24, 25]. A negative silicon wafer master was made using a two-step Deep Reactive Ion Etching (DRIE) process. Two different etching depths were obtained by subsequently applying two masks to the same wafer. A mask with 10x10 mm arrays with circles of 2 µm diameter and 4 µm center-to-center distance in a hexagonal grid was used as a negative for the micropillar arrays and a mask with two rectangular spacers of 10x2 mm was aligned on the sides of the arrays. The etching depth was varied for the micropillar arrays to make short and long pillars, calculated to have a bending stiffness of 66 nN/µm and 16 nN/µm, respectively using finite element modeling [25]. Using a published elastic model [26], we calculated that these bending stiffnesses corresponded to a Young's modulus in continuous (e.g. PAA) substrates of approximately 47.2 and 11.6 kPa; corresponding to a shear modulus of 15.7 and 3.87 kPa, respectively. The etching depth of the spacers was set to 50 µm, to enable high-resolution microscopy with inverted micropillar arrays (see microscopy).

After passivation of the negative silicon master with trichloro silane (Sigma Aldrich), well-mixed PDMS at 1:10 (crosslinker:prepolymer) ratio was poured over the wafer. After 20 hours at 110°C, the PDMS was

fully cured at a stiffness of 2.5 MPa (as determined by tensile testing). The individual micropillar arrays were peeled off with two spacers on the sides. ECM stamping was performed using a flat piece of PDMS (1:30 ratio, cured 16 hours at 65°C). Per stamp, a 40 µL mix of 50 µg/mL unlabeled fibronectin (Sigma Aldrich) and 10 µg/mL Alexa405 or Alexa647 (both from Invitrogen)-conjugated fibronectin was used. After stamping, the micropillars were blocked with 0.2% Pluronic (F-127, Sigma Aldrich) in PBS for 1 hour at room temperature and washed with PBS.

Cells were seeded either in complete medium, serum-free medium or medium containing blocking antibodies targeting mouse integrin αv subunit and imaging of F-actin and labeled fibronectin was performed after cell spreading. For some analyses, after cell spreading the medium was exchanged for medium containing 0.25 or 0.5 µM Y27632 Rho kinase inhibitor (Tocris cat.#1254, Bristol, UK); 50 µM blebbistatin Myosin-II inhibitor (Calbiochem cat. #203389, Merck KGaA, Darmstadt, Germany); or 0.5 µM Latranculin B F-actin polymerization inhibitor (Calbiochem cat. #428020) and further incubated for 1 hour followed by 4% formaldehyde fixation and immunostaining.

### 3.4.9 Immunostaining

Cells were fixed in 4% formaldehyde and then permeabilized with 0.1% Triton-X and 0.5% BSA in PBS. Immunostaining was performed for (pY188) Paxillin (Biosource/Invitrogen cat. # 44-722G; Becton Dickinson cat# 610052) followed by secondary antibodies conjugated with Alexa488 (Invitrogen / Fisher Scientific cat# A11008) or Alexa647 (Jackson ImmunoResearch cat# 115-605-006). Rhodamine-Phalloidin (Sigma-Aldrich cat. # 77418-1EA) or Alexa 568-Phalloidin (Fisher Emergo B.V. cat. # A12380, Thermo Fisher) was used to stain F-actin. Hoechst 33258 was used to visualize nuclei.

### 3.4.10 Microscopy

High-resolution imaging was performed on an in-house constructed setup based on an Axiovert200 microscope body (Zeiss, Sliedrecht, The Netherlands). Confocal imaging was achieved by means of a spinning disk unit (CSU-X1, Yokogawa, Amersfoort, The Netherlands). The confocal image was connected to an emCCD camera (iXon 897, Andor, Belfast, UK). IQ-software (Andor) was used for basic setup-control and data acquisi-

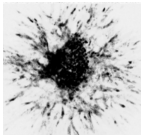

tion. Three laser lines were coupled through a polarization-maintaining single-mode fiber, controlled using an Acousto-Optical Tunable Filter (AA Optoelectronics, Orsay, France): 405 nm (Crystalaser, Reno, NV, USA), 488 nm (Coherent, Santa Clara, CA, USA) and 561 nm (Cobolt, Stockholm, Sweden). Incorporated 50 µm spacers next to the micropillar arrays combined with a 100 µm thick coverslip enabled the use of a high numerical-aperture (1.4) objective with 100X magnification. For live cell imaging and imaging of 3T3 cells; Nikon Eclipse Ti microscope in scanning confocal mode was used together with 20x magnification 0.75NA dry air lens with internal 1.5x magnification and 4.184 scanner zoom to obtain a pixel size of 0.2 µm.

### 3.4.11 Image analysis

All image analysis was performed using specifically designed Matlab scripts (Mathworks, Natick, MA, USA). For cell area analysis scripts generated by Hans de Bont (Division of Toxicology, Leiden Academic Center for Drug Research, Leiden, the Netherlands) were adapted to apply a rolling ball filter to the image followed by a median filter and subsequently cell detection and image segmentation was performed manually per image to best obtain area per single cell.

For cell-matrix adhesion analysis a cell mask was generated by passing the image of the actin channel through a Gaussian low pass filter. Subsequently, the background intensity was subtracted and the image was run through a sobel and a log-edge detection algorithm followed by image dilation and hole filling each time. The outputs were checked and new masks were generated manually as described above when the mask did not correctly correspond to the cell. Subsequently, for cell-matrix adhesion detection, pY188 Paxillin signal that was assigned to a cell within 20 µm from the cell border was first passed through a Gaussian low pass filter, and signal that was 4 standard deviations larger than the average of the signal was assigned to cell-matrix adhesions. The binary adhesion images were then subjected to a hole-filling algorithm followed by watershed segmentation. The results were manually checked and images showing incorrect adhesion recognition due to low signal-to-noise ratio were excluded from analysis.

For the actin filament analysis, a rolling ball filter was applied to the actin signal inside the cell mask area. Then the signal one standard deviation above the mean was taken as foreground signal. To re-

move noise from the signal, the signal was shrunk, then singular pixels were removed and finally the image was dilated once. From this image, objects smaller than 0.2 µm$^2$ were removed and then the image was skeletonized followed by connecting diagonals to connect neighboring filaments and then removing all branching points to analyze filaments separately. When analyzing cortical actin, only filaments within 2 µm of the cell border were taken into account. For orientation analysis, all filaments were averaged over all cells and the output was convolved with a unit Gaussian to improve the visualization. This was then corrected for square imaging window by calculating the maximum measurable fiber length in a given angle and weighing this correction per stretch condition by the percentage of a cell of measured average size falling outside of the imaging window if it was circle (Figure S2E).

### 3.4.12 Pillar deflection analysis

Pillar deflections were determined with approximately 30 nm precision using a specifically designed Matlab script [25]. Briefly, the exact pillar locations were determined from the labeled fibronectin fluorescence image using a fit to the cross-correlation function between a perfect binary circle and the local fluorescence of one pillar. The undeflected hexagonal grid was determined and used as reference to the determined pillar locations. The precision of the forces was pillar bending stiffness dependent, where the high- and low stiffness pillars had a precision of 2 nN and 0.5 nN, respectively.

Cell masks were generated using the same algorithm as cell-matrix adhesion analysis that was then dilated. The pillars under this dilated image that had a deflection larger than 0.06 µm for fixed and integrin blocking assay and larger than 0.2 µm for all other live assays were taken for analysis. Total force was calculated by adding all the absolute deflections and multiplying it by the bending stiffness. The centripetal force percentage was obtained by dividing the radial components of the forces (the forces that point towards the center of the generated cell mask) by the total cellular force.

### 3.4.13 Statistical analysis

To calculate significance between two conditions, the Mann-Whitney U test was used. To quantify the PAA substrate responses, a cumulative

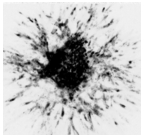

Gaussian distribution was fitted to the data and the half response point (the mean of the distribution) was compared between the conditions using the F-test in the GraphPad Prism 6 program (GraphPad Software, La Jolla, CA, USA).

## 3.5 Acknowledgements

We thank O. Pertz for providing the mCherry-LifeAct construct; W. Pomp and D. Civita for assistance in setting up cyclic stretcher; K.A. Jansen and G.H. Koenderink for their help in characterizing PAA gels; and H. De Bont for assistance with image analysis. **Funding:** Support for this work came from the Netherlands Organization for Scientific Research (FOM 09MMC03 and 09MMC01). **Author contributions:** H.E.B. performed the experiments. H.E.B., H.v.H., D.M.D., T.S., and E.H.J.D. designed the experiments and analyzed and interpreted data. H.E.B. and E.H.J.D wrote the manuscript. **Competing interests:** The authors declare no competing interests.

## 3.6 Supplemental figures

### Figure S1

***Integrin and mCherry-LifeAct expression measurements using FACS.*** *(A,B) Human integrin β1 and integrin β3 expression levels for GDβ1 (A) and GDβ3 cells (B). (C-F) Human integrin β1, human integrin β3 and mCherry-LifeAct expression levels for either wild type(C,D) or mCherry-LifeAct expressing (E,F) GEβ1 (C,E) and GEβ3 (D,F) cells. (G,H) Human integrin β1 (left) and human integrin β3 (right) expression levels in GEβ1 (blue), GEβ3 (red) (G) or GDβ1 (blue) and GDβ3 (red) (H) compared to expression of these integrins in the human breast cancer cell line MDA-MB-435s (green). (I,J) Quantification of percentage of cells that are integrin positive, i.e. falls in P2 gate indicated at A-F (I), or positive for mCherry-LifeAct expression, i.e. falls in P3 gate indicated at C-F (J). Mean and standard deviation are shown of three independent experiments for I and J.*

### Figure S2

***Strain field of cyclic stretcher, characterization of PAA gels with bulk rheology and integrin-mediated cell adhesion to PAA and PDMS substrates.*** *(A) Magnified homogeneous displacement field under static strain over the entire substrate of 8x10 mm (height x width). Global strain is applied over the x-axis and the net strain from differentiation over this field is homogeneous. (B) Positions of fluorescent beads at the minimal and maximal strain during 10% (top) or 20% (bottom) cyclic stretch measured manually and calculated strain (calculations of only point 0 reference is shown, mean and deviation are obtained by taking all points as reference one by one). (C) Representation of how the length "r" and orientation angle "A" of a filament would change under a horizontal and vertical strain of εx and εy, respectively to a length of r' and an angle of A'. (D) Analytical calculation of minimal strain direction, finding A where r'(A')=r(A), for measured strain values (B). (E) Correction factor for square imaging window where A is the angle, C is the cell size (obtained from Figure 1D) and L is the imaging window length (69 μm for this experiment). The cosine/sine term in the denominator is due to the variation in maximum measurable fiber length in a given angle and the nominator is the portion of a cell of measured size falling outside of the imaging window if the imaging window was a circle with diameter L. (F) Shear storage modulus of a PAA gel of 7.5% acrylamide and 0.2% bis-acrylamide during polymerization and its temperature dependence. (G) The final shear elastic modulus measured at 37°C for PAA gels with varying bis-acrylamide concentration. Each bar represents a separate experiment performed on different days and using two different rheometers. (H,I) Adhesion to 1:10 (crosslinker:prepolymer) ratio PDMS (H) and 12.2 kPa PAA (I) of GEβ1 and GEβ3 cells preincubated with- and seeded in the absence or presence of integrin blocking antibodies targeting mouse-αv, mouse-α5, human-β1 or human-β3.*

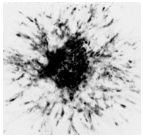

## Figure S3

***Average cell-matrix adhesion area remains constant with increasing stiffness.*** *(A) Cumulative Gaussian distribution and Gaussian distribution functions used to obtain the fit parameters for cell spreading and cell matrix adhesion formation. (B) The fit parameters obtained by fitting cumulative Gaussian distribution model and the p values obtained by comparing the indicated fit parameters between β1 and β3 expressing cells using the F-test. (C-F) Slopes of the fits shown in figures 2A,B and 3A,B describing stiffness-dependent induction of cell spreading (C,D) and peripheral cell matrix adhesion formation (E,F) as a function of substrate rigidity at the stiffness range tested. (G,H) Quantification of average size of peripheral cell-matrix adhesions of GEβ1 and GEβ3 cells (G) or GDβ1 and GDβ3 (H) for cells with at least 10 adhesions. In all graphs, mean ±95% clearance level is shown and at least 20 cells were measured over 3 different experiments (except for 760 Pa for GEβ1 and GEβ3 cells where results of one experimental replica is shown). P values were calculated by comparing the slope of the linear fits with F-test. (I,J) Representative images of Paxillin staining for GDβ1 (I) and GDβ3 cells (J). Upper row shows raw immunofluorescence staining, middle row shows zoomed in region of the boxed area, and bottom row shows adhesions detected by the automated analysis algorithm. Scale bar is 20 µm (5 µm for zooms).*

## Figure S4

***Increased cellular traction force in response to substrate stiffening is maintained in post-fixation samples and antibody blocking confirms role for αv integrins in force exertion by GEβ3 but not by GEβ1 cells.*** *(A,B) Bar plots of cellular spread area (A) and force per pillar (B) measured in fixed GEβ1, GEβ3, GDβ1, GDβ3 and NIH-3T3 cells on 6.9 and 4.1 µm pillars. In A,B mean ±95% clearance level is shown and at least 15 cells were measured from three independent experiments. (C) Representative images from A,B. (D,E) Bar plots of cellular spread area (D) and force per pillar (E) analyzed by live cell imaging of mCherry-LifeAct-expressing GEβ1 and GEβ3 cells seeded on 4.1 µm pillars for 5 hours in the presence or absence of blocking antibody against mouse integrin αv. In D,E mean ±95% clearance level is shown and at least 50 cells were measured from a single experiment. NS, $p>0.05$; **, $p<0.005$; ***, $p<0.0005$ compared to control according to Mann-Whitney test. (F) Representative images of D,E. White arrows indicate magnitude and direction of forces measured. Scale bar, 20 nN/10 µm.*

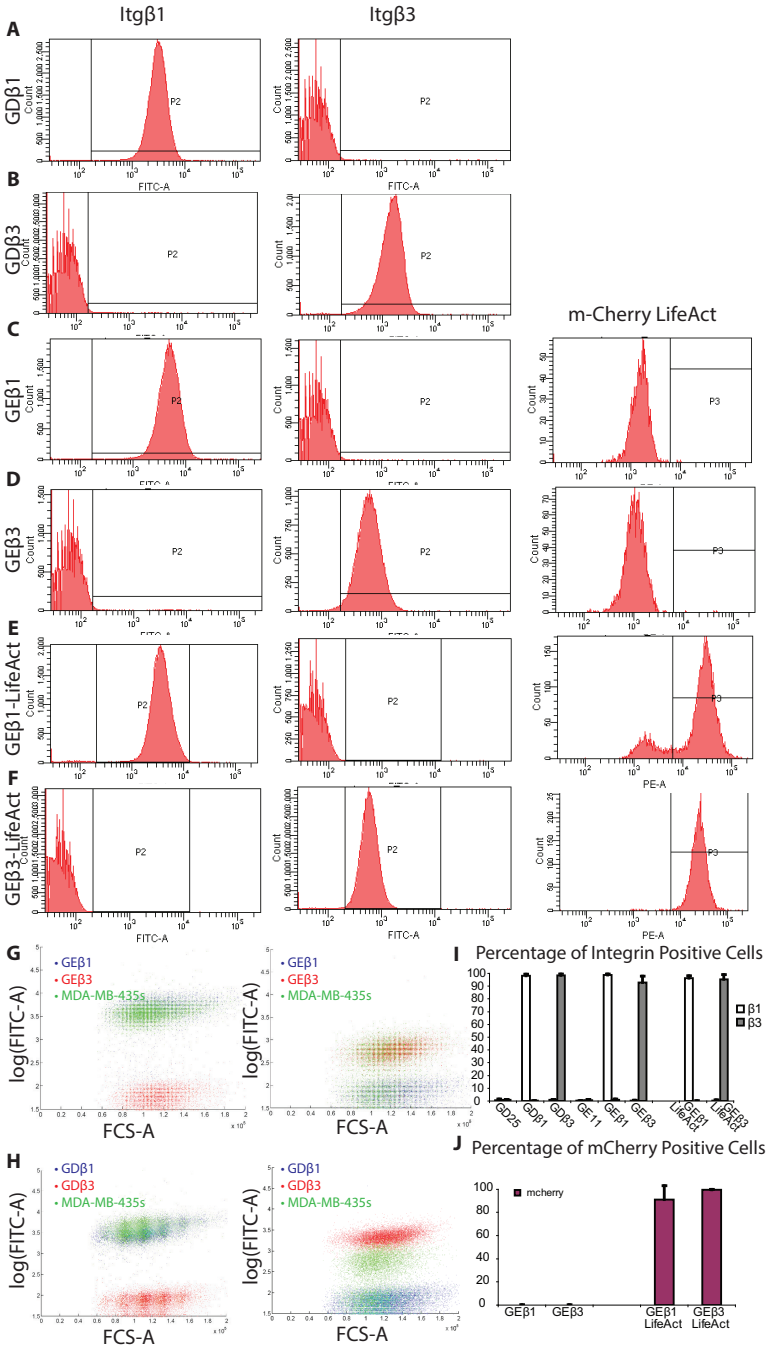


**Figure S1**
***Integrin and mCherry-LifeAct expression measurements using FACS.***

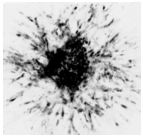

A

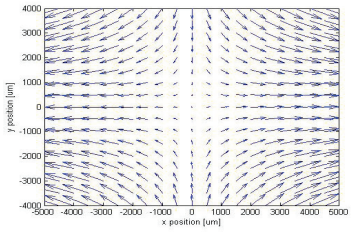


B

| 10% stretch | absolute positions before stretch | | absolute positions after stretch | | reference from point 0 before stretch | | reference from point 0 after stretch | | strain when dx(or dy)>100 | |
|---|---|---|---|---|---|---|---|---|---|---|
| | x | y | x | y | dx | dy | dx | dy | dcx | dcy |
| point 0 | 208 | 372 | 183 | 382 | 0 | 0 | 0 | 0 | | |
| point 1 | 131 | 439 | 100 | 445 | -77 | 67 | -83 | 63 | | |
| point 2 | 392 | 285 | 380 | 298 | 184 | -87 | 197 | -84 | 1.0707 | |
| point 3 | 163 | 144 | 133 | 160 | -45 | -228 | -50 | -222 | | 0.9737 |
| point 4 | 431 | 437 | 424 | 445 | 223 | 65 | 241 | 63 | 1.0807 | |
| point 5 | 494 | 332 | 491 | 342 | 286 | -40 | 308 | -40 | 1.0769 | |
| point 6 | 185 | 99 | 159 | 119 | -23 | -273 | -24 | -263 | | 0.9634 |
| point 7 | 313 | 86 | 299 | 105 | 105 | -286 | 116 | -277 | 1.1048 | 0.9685 |
| point 8 | 174 | 31 | 146 | 52 | -34 | -341 | -37 | -330 | | 0.9677 |
| point 9 | 400 | 67 | 390 | 87 | 192 | -305 | 207 | -295 | 1.0781 | 0.9672 |
| point 10 | 66 | 215 | 31 | 230 | -142 | -157 | -152 | -152 | 1.0704 | 0.9682 |
| point 11 | 415 | 494 | 409 | 499 | 207 | 122 | 226 | 117 | 1.0918 | 0.959 |
| | | | | | | | | mean | 1.0806 | 0.9654 |
| | | | | | | | | std | 0.0105 | 0.0053 |

| 20% stretch | absolute positions before stretch | | absolute positions after stretch | | reference from point 0 before stretch | | reference from point 0 after stretch | | strain when dx(or dy)>100 | |
|---|---|---|---|---|---|---|---|---|---|---|
| | x | y | x | y | dx | dy | dx | dy | dcx | dcy |
| point 0 | 401 | 64 | 316 | 190 | 0 | 0 | 0 | 0 | | |
| point 1 | 214 | 123 | 102 | 246 | -187 | 59 | -214 | 56 | 1.1444 | |
| point 2 | 265 | 314 | 158 | 424 | -136 | 250 | -158 | 234 | 1.1618 | 0.936 |
| point 3 | 400 | 365 | 314 | 475 | -1 | 301 | -2 | 285 | | 0.9468 |
| point 4 | 232 | 246 | 127 | 363 | -169 | 182 | -189 | 173 | 1.1183 | 0.9505 |
| point 5 | 163 | 259 | 43 | 374 | -238 | 195 | -273 | 184 | 1.1471 | 0.9436 |
| point 6 | 465 | 345 | 385 | 453 | 64 | 281 | 69 | 263 | | 0.9359 |
| point 7 | 242 | 18 | 133 | 144 | -159 | -46 | -183 | -46 | 1.1509 | |
| point 8 | 317 | 314 | 217 | 427 | -84 | 250 | -99 | 237 | | 0.948 |
| point 9 | 315 | 202 | 218 | 321 | -86 | 138 | -98 | 131 | | 0.9493 |
| point 10 | 495 | 312 | 429 | 428 | 94 | 248 | 113 | 238 | | 0.9597 |
| point 11 | 370 | 156 | 280 | 275 | -31 | 92 | -36 | 85 | | |
| | | | | | | | | mean | 1.1445 | 0.9499 |
| | | | | | | | | std | 0.022 | 0.0129 |

C

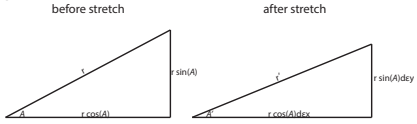


D

$$r' = \sqrt{(r\cos(A)d\varepsilon x)^2 + (r\sin(A)d\varepsilon y)^2} = r^2\sqrt{\cos^2(A)d\varepsilon x^2 + \sin^2(A)d\varepsilon y^2}$$

For minimal strain $\frac{r'}{r} = 1$ hence $\sqrt{\cos^2(A)d\varepsilon x^2 + \sin^2(A)d\varepsilon y^2} = 1$

For 10% stretch we measured $d\varepsilon x = 1.08 \pm 0.01$ and $d\varepsilon y = 0.965 \pm 0.005$

And for 20% stretch we measured $dx = 1.14 \pm 0.02$ and $dy = 0.95 \pm 0.01$

$$\sqrt{\cos^2(A)(1.08)^2 + \sin^2(A)(0.965)^2} = 1$$
$$1.166\cos^2(A) + 0.931\sin^2(A) = 1$$
$$0.166\cos^2(A) - 0.069\sin^2(A) = 0 \quad \Rightarrow \quad \tan^2(A) = 2.406$$
$$A = 57.2^0$$

$$\sqrt{\cos^2(A)(1.14)^2 + \sin^2(A)(0.95)^2} = 1$$
$$1.300\cos^2(A) + 0.903\sin^2(A) = 1$$
$$0.300\cos^2(A) - 0.097\sin^2(A) = 0 \quad \Rightarrow \quad \tan^2(A) = 3.093$$
$$A = 60.4^0$$

E

$$f(A,C) = \frac{\left(1 + \frac{2}{L}\sqrt{\frac{C}{\pi}}\right)^2 - 1}{\cos(A)} + 1 \quad for\ A < 45^\circ\ and\ \ f(A,C) = \frac{\left(1 + \frac{2}{L}\sqrt{\frac{C}{\pi}}\right)^2 - 1}{\sin(A)} + 1 \quad for\ A > 45^\circ$$

F

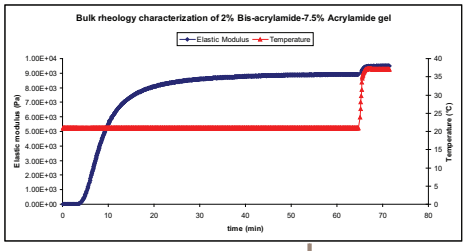


G

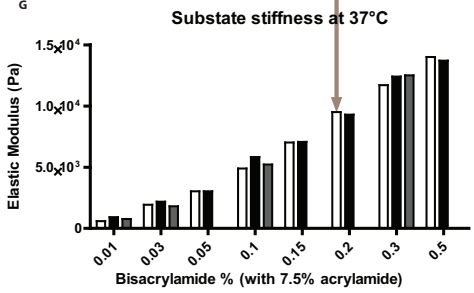


H

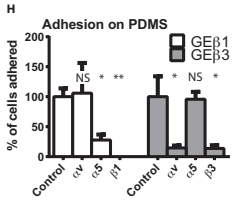


I

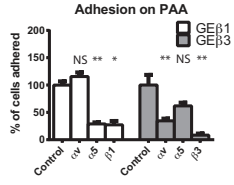


## Figure S2

***Strain field of cyclic stretcher, characterization of PAA gels with bulk rheology and integrin-mediated cell adhesion to PAA and PDMS substrates.***

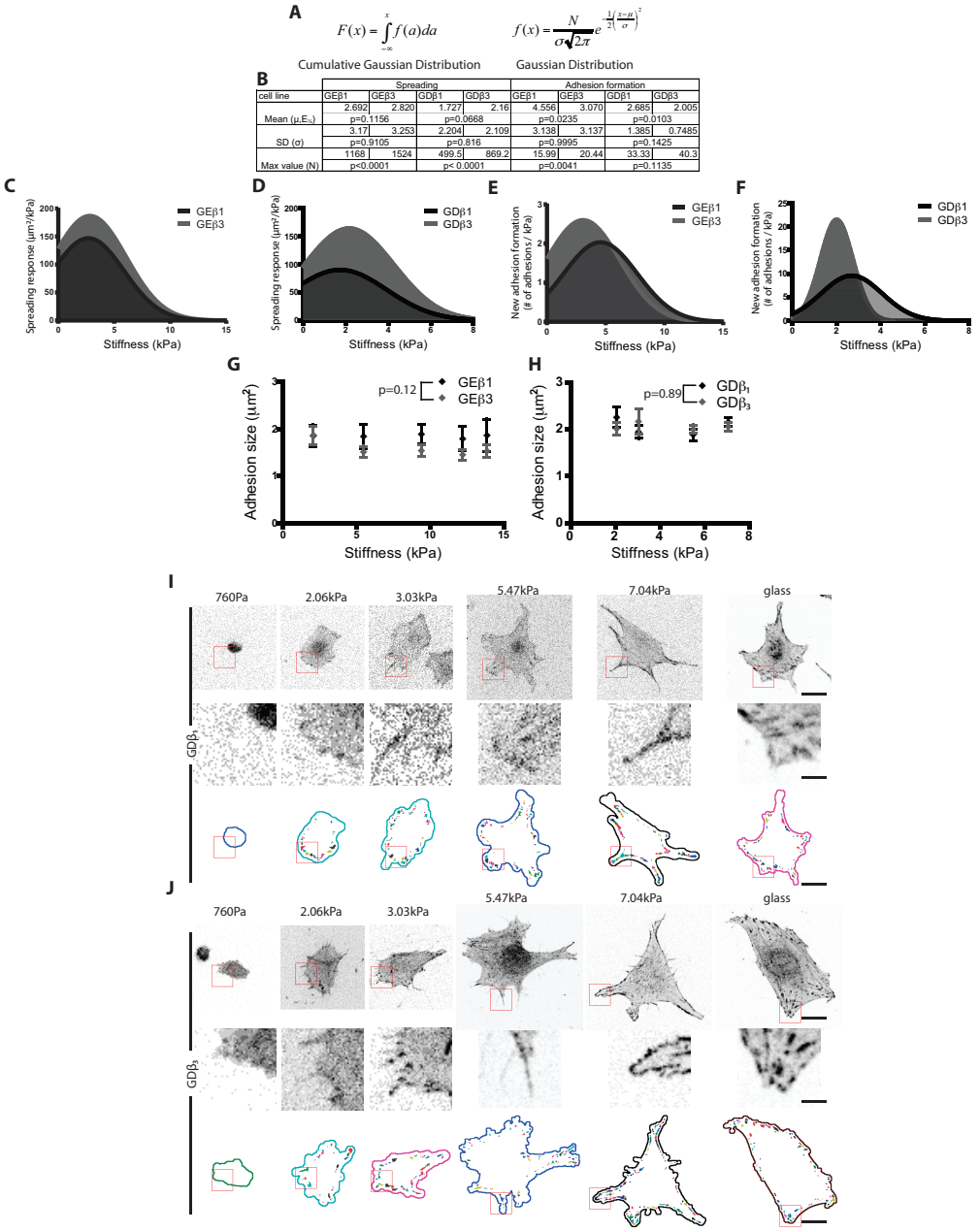


**Figure S3**

***Average cell-matrix adhesion area remains constant with increasing stiffness.***

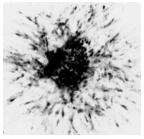

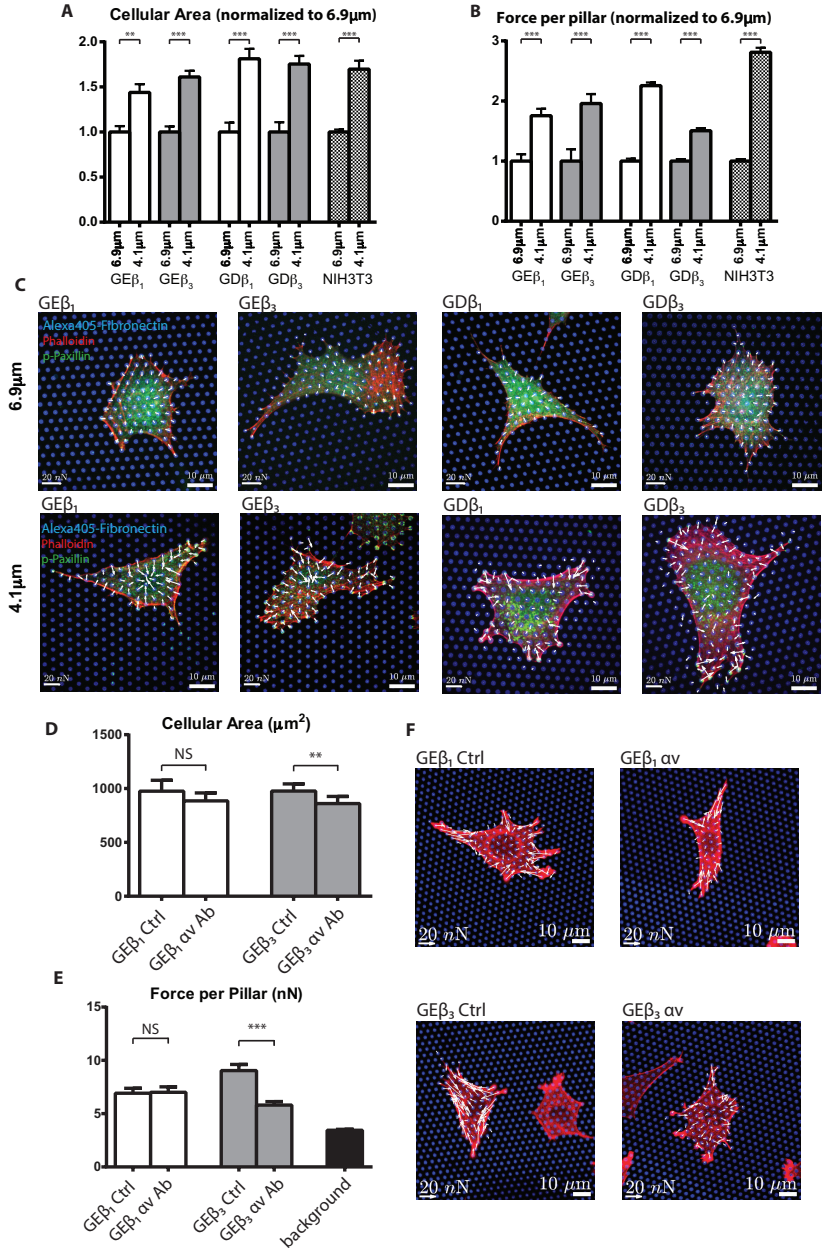


## Figure S4

***Increased cellular traction force in response to substrate stiffening is maintained in post-fixation samples and antibody blocking confirms role for αv integrins in force exertion by GEβ3 but not by GEβ1 cells.***

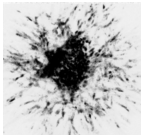

# Bibliography


[1] Brenton D Hoffman, Carsten Grashoff, and Martin A Schwartz. "Dynamic molecular processes mediate cellular mechanotransduction". In: *Nature* 475.7356 (2011).

[2] Herbert B Schiller and Reinhard Fässler. "Mechanosensitivity and compositional dynamics of cell-matrix adhesions". In: *EMBO Reports* 14.6 (2013).

[3] Richard O Hynes. "Integrins: Bidirectional, allosteric signaling machines". In: *Cell* 110.6 (2002).

[4] Daniel Choquet, Dan P Felsenfeld, and Michael P Sheetz. "Extracellular matrix rigidity causes strengthening of integrin-cytoskeleton linkages". In: *Cell* 88.1 (1997).

[5] Julie C Friedland, Mark H Lee, and David Boettiger. "Mechanically Activated Integrin Switch Controls alpha(5)beta(1) Function". In: *Science (New York, N.Y.)* 323.5914 (2009).

[6] Christophe Guilluy et al. "The Rho GEFs LARG and GEF-H1 regulate the mechanical response to force on integrins". In: *Nature Cell Biology* 13.6 (2011).

[7] Pere Roca-Cusachs, Thomas Iskratsch, and Michael P. Sheetz. "Finding the weakest link - exploring integrin-mediated mechanical molecular pathways". In: *Journal of Cell Science* 125.13 (2012).

[8] Daniel Bouvard et al. "Integrin inactivators: balancing cellular functions in vitro and in vivo". In: *Nature Reviews Molecular Cell Biology* 14.7 (2013).

[9] Haguy Wolfenson, Irena Lavelin, and Benjamin Geiger. "Dynamic Regulation of the Structure and Functions of Integrin Adhesions". In: *Developmental Cell* 24.5 (2013).

[10] Jay S Desgrosellier and David A Cheresh. "Integrins in cancer: biological implications and therapeutic opportunities". In: *Nature Reviews Cancer* 10.1 (2010).

[11] Erik HJ Danen et al. "The fibronectin-binding integrins alpha5beta1 and alphavbeta3 differentially modulate RhoA-GTP loading, organization of cell matrix adhesions, and fibronectin fibrillogenesis". In: *Journal of Cell Biology* 159.6 (2002).

[12] Erik HJ Danen et al. "Integrins control motile strategy through a Rho-cofilin pathway". In: *Journal of Cell Biology* 169.3 (2005).

[13] Hui Miao et al. "Differential regulation of Rho GTPases by beta 1 and beta 3 integrins: the role of an extracellular domain of integrin in intracellular signaling". In: *Journal of Cell Science* 115.10 (2002).

[14] Dominic P White, Patrick T Caswell, and Jim C Norman. "alpha-v beta-3 and alpha-5 beta-1 integrin recycling pathways dictate downstream Rho kinase signaling to regulate persistent cell migration". In: *Journal of Cell Biology* 177.3 (2007).

[15] Stephan Huveneers et al. "Binding of soluble fibronectin to integrin alpha 5 beta 1 - link to focal adhesion redistribution and contractile shape". In: *Journal of Cell Science* 121.15 (2008).

[16] Pere Roca-Cusachs et al. "Clustering of alpha(5)beta(1) integrins determines adhesion strength whereas alpha(v)beta(3) and talin enable mechanotransduction". In: *Proceedings of the National Academy of Sciences of the United States of America* 106.38 (2009).

[17] Herbert B Schiller et al. "beta(1)- and alpha(v)-class integrins cooperate to regulate myosin II during rigidity sensing of fibronectin-based microenvironments". In: *Nature Cell Biology* 15.6 (2013).

[18] Douglas Woods et al. "Induction of beta 3-integrin gene expression by sustained activation of the Ras-regulated Raf-MEK-extracellular signal-regulated kinase signaling pathway". In: *Molecular and Cellular Biology* 21.9 (2001).

[19] Gordon B Mills and Wouter H Moolenaar. "The emerging role of lysophosphatidic acid in cancer". In: *Nature Reviews Cancer* 3.8 (2003).

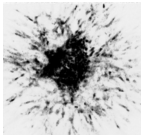

[20] Akira Katsumi et al. "Integrin activation and matrix binding mediate cellular responses to mechanical stretch". In: *Journal of Biological Chemistry* 280.17 (2005).

[21] Grace L Lin et al. "Activation of beta 1 but not beta 3 integrin increases cell traction forces". In: *FEBS Letters* 587.6 (2013).

[22] Tony Yeung et al. "Effects of substrate stiffness on cell morphology, cytoskeletal structure, and adhesion". In: *Cell Motility and the Cytoskeleton* 60.1 (2005).

[23] Karin A Jansen et al. "Cells Actively Stiffen Fibrin Networks by Generating Contractile Stress". In: *Biophysical Journal* 105.10 (2013).

[24] Lea Trichet et al. "Evidence of a large-scale mechanosensing mechanism for cellular adaptation to substrate stiffness". In: *Proceedings of the National Academy of Sciences of the United States of America* 109.18 (2012).

[25] Hedde van Hoorn et al. "The Nanoscale Architecture of Force-Bearing Focal Adhesions". In: *Nano Letters* 14.8 (2014).

[26] Marion Ghibaudo et al. "Traction forces and rigidity sensing regulate cell functions". In: *Soft Matter* 4.9 (2008).